Gene expression map of the *Arabidopsis* shoot apical meristem stem cell niche

Ram Kishor Yadav, Thomas Girke, Sumana Pasala, Mingtang Xie, and G. Venugopala Reddy[1]

Center for Plant Cell Biology and Department of Botany and Plant Sciences, 2150 Batchelor Hall, University of California, Riverside, CA 92521.

Communicated by Elliot M. Meyerowitz, California Institute of Technology, Pasadena, CA, January 27, 2009 (received for review December 9, 2008)

Despite the central importance of stem cells in plant growth and development, the molecular signatures associated with them have not been revealed. Shoot apical meristems (SAMs) harbor a small set of stem cells located at the tip of each plant and they are surrounded by several million differentiating cells. This imposes a major limitation in isolating pure populations of stem cells for genomic analyses. We have developed a system to isolate pure populations of distinct cell types of the SAMs, including stem cells. We have used this system to profile gene expression from 4 different cell samples of SAMs. The cell sample-specific gene expression profiling has resulted in a high-resolution gene expression map to reveal gene expression networks specific to individual spatial domains of SAMs. We demonstrate that the cell sample-specific expression profiling is sensitive in identifying rare transcripts expressed in a few specific subsets of cells of SAMs. Our extensive RNA in situ analysis reveals that the expression map can be used as a predictive tool in analyzing the spatial expression patterns of genes and it has led to the identification of unique gene expression patterns within the SAMs. Furthermore, our work reveals an enrichment of DNA repair and chromatin modification pathways in stem cells suggesting that maintenance of genome stability and flexible chromatin may be crucial for stem cell function. The gene expression map should guide future reverse genetics experiments, high-resolution analyses of cell–cell communication networks and epigenetic modifications.

central zone | CLAVATA3 | fluorescence-activated cell sorting | WUSCHEL

Spatiotemporal regulation of transcriptional programs mediated by cell–cell communication networks is crucial in stem cell maintenance (1, 2). Understanding the complexity of transcriptional programs requires a high resolution analysis of gene expression, preferably at a cell type-specific resolution (3). Shoot apical meristems (SAMs) of higher plants represent a dynamic and interconnected network of distinct cell types. In *Arabidopsis thaliana*, the SAM consists of ≈35 stem cells, located within the central zone (CZ) (4). Stem cells are surrounded by several million differentiating cells that are part of the adjacent peripheral zone (PZ) and developing organs. The cells of the Rib-meristem (RM) that are located just beneath the CZ provide positional cues necessary for stem cell maintenance (Fig. 1 *D* and *E*). Earlier studies have revealed molecular mechanisms involved in stem cell maintenance (5). However, gene networks that underlie the stem cell maintenance process are far from understood. The development of high resolution gene expression map of distinct cell types of SAMs could enable network analysis of pathways involved in stem cell maintenance.

Expression profiling studies of specific cell types have been performed on *Arabidopsis* root system (3, 6), however, studies on the SAMs have been restricted to experiments of the entire tissue (7). This is because the domains of specific cell types of the SAMs are extremely small. For example, the stem cell domain marked by the expression of the only available marker, *pCLAVATA3*(*CLV3*)::*mGFP5-ER* [*CLAVATA3* promoter attached to the endoplasmic reticulum localized-GFP], has revealed that there are only ≈35 stem cells within a SAM (Fig. S1 *A* and *C*). This imposes a limitation in isolating sufficient amounts of specific cell types for expression profiling (4). In this study, we have used *apetala1-1;cauliflower1-1* (*ap1-1;cal1-1*) double mutant background to isolate fluorescently-labeled protoplasts from 4 distinct cell samples of SAMs. A single *ap1-1;cal1-1* double mutant plant can produce up to several hundred SAMs owing to the conversion of floral meristem identity into inflorescence meristem identity, thereby providing primary enrichment of SAM tissue (Fig. 1 *G–I*) (8). The expression profiling of transcripts from 4 different cell populations and informatics analysis has revealed gene expression networks specific to different spatial domains of the stem cell niche. We demonstrate that the expression profiling method is sensitive in identifying rare transcripts expressed in a few specific subsets of SAMs. Our extensive RNA in situ analysis reveals that the expression map can be used as a predictive tool in analyzing the expression patterns of unknown genes (Fig. S2). Our work also reveals an enrichment of DNA repair and chromatin modification pathways in stem cells implying that maintenance of genome stability and flexible chromatin may be crucial for stem cell function.

Results and Discussion

Gene Expression and Cell–Cell Communication Machinery in *ap1-1;cal1-1* System. We tested whether *ap1-1;cal1-1* SAMs are suitable for cell type specific expression profiling by analyzing the organization of the CZ and the RM. The expression patterns of *CLV3,* and *WUSCHEL* (*WUS*), markers for the cells of the CZ and the RM respectively, were visualized by whole mount RNA in situ analysis. This allowed us to demonstrate that the expression patterns of *CLV3* and *WUS* are similar to the WT expression patterns observed in previous studies (Fig. S1 *A* and *B*) (9, 10). Furthermore, we tested whether the *ap1-1;cal1-1* SAMs are comparable to WT SAMs with respect to the CLV-WUS-mediated intercellular communication process. Mutations in *clv3* gene result in expansion of the CZ. CLAVATA3 (CLV3), a small extracellular protein synthesized in the CZ activates CLAVATA1 (CLV1)-CLAVATA2 (CLV2) receptor kinase complex in RM cells (5). The active CLV1-CLV2 receptor kinase complex functions by down regulating the expression of WUSCHEL (WUS), a homeodomain protein expressed in RM cells. An earlier live-imaging study has revealed that the transient silencing of the *CLV3* gene results in an increased *CLV3* promoter activity in the native domain within 24 h of *CLV3* silencing and followed by the radial expansion of the CZ in the next 48 h. We tested whether a similar CZ reorganization pattern could be observed in the SAMs of *ap1-1;cal1-1* plants. The live-imaging of SAMs of *ap1-1;cal1-1* mutants, upon *CLV3* silencing, revealed a similar temporal sequence of CZ expansion that was observed in WT SAMs (4). This suggested that the intercellular communication-mediated by CLV-WUS network is operational in *ap1-1;cal1-1* SAMs (Fig. S1 *C* and *D*). Therefore, we adapted a protoplasting method, followed by FACS analysis to isolate fluorescently-labeled cell populations of distinct cell types from *ap1-1;cal1-1* SAMs (11) (*SI Text*).

Author contributions: R.K.Y., S.P., M.X., and G.V.R. performed research; R.K.Y., T.G., and G.V.R. analyzed data; R.K.Y., T.G., and G.V.R. wrote the paper; G.V.R. designed research.

The authors declare no conflict of interest.

[1]To whom correspondence should be addressed. E-mail: venug@ucr.edu.

This article contains supporting information online at www.pnas.org/cgi/content/full/0900843106/DCSupplemental.

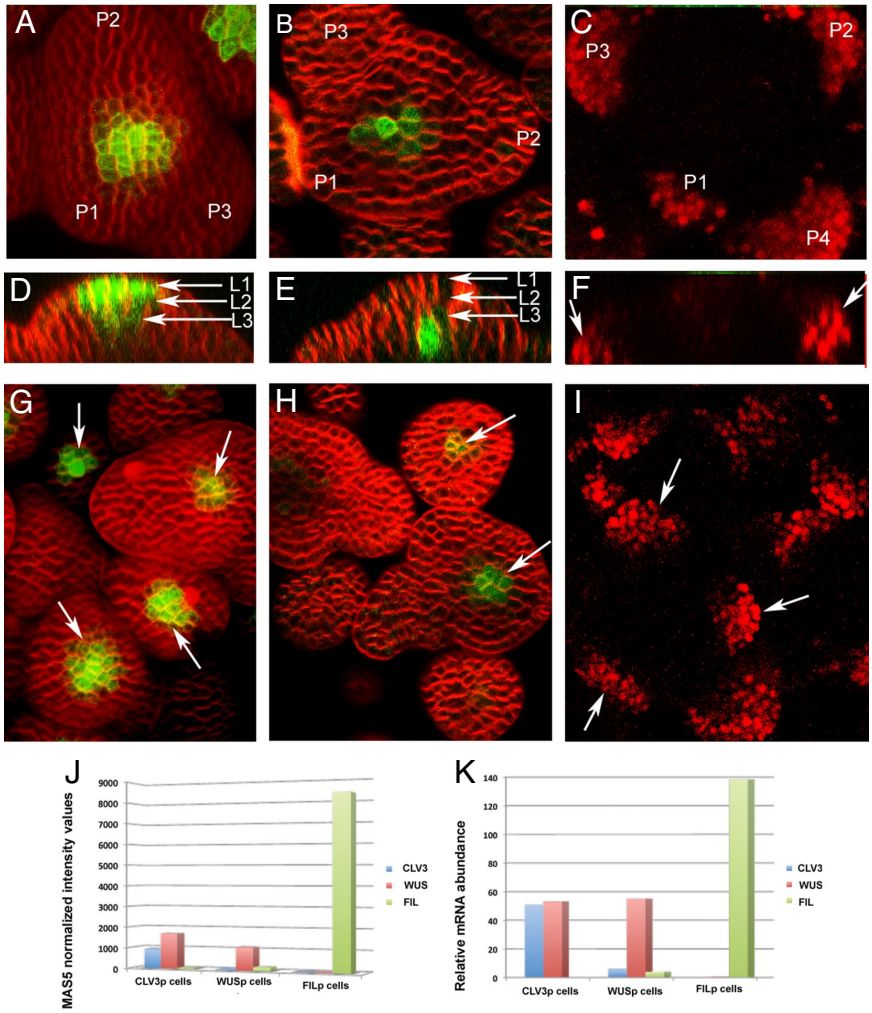

Fig. 1. Expression patterns of 3 marker lines of shoot apical meristems. (*A*) A 3D view of WT SAM labeled with FM4–64 (red) and *pCLV3*::*mGFP5-ER* (green), a marker for the central zone (CZ). (*B*) An optical section depicting *pWUS*::*mGFP5-ER* expression (green) and FM4–64 (red) in the WT SAM. (*C*) A 3D-view of WT SAM expressing *pFIL*::*Ds-Red-N7* (red), marking the organ primordia. (*D*) A side-view of (*A*) exhibiting the *pCLV3*::*mGFP5-ER* expression extending up to the 4th cell layer from the tip. (*E*) A side-view of *B*, depicting the expression pattern of *pWUS*::*mGFP5-ER* (green) in the L3 layer (arrows) and cell layers located beneath. (*F*) A side-view of *C*, exhibiting the expression pattern of *pFIL*::*Ds-Red-N7* (Red) (arrows). (*G*) A 3D-view of *ap1-1;cal1-1* SAM labeled with FM4–64 (red) and *pCLV3*::*mGFP5-ER* (green) marking the CZ (arrows). (*H*) A horizontal sections of *ap1-1;cal1-1* SAM expressing *pWUS*::*mGFP5-ER* (green) is labeled with FM4–64 (Red) depicting the expression of *WUS* in the RM (arrows). (*I*) A 3D view of the *ap1-1;cal1-1* SAM exhibiting the expression of *pFIL*::*Ds-Red* (Red) marking the primordia in the shoot apex (arrows). (*J*) A comparison of MAS5-normalized microarray intensity values of 3 genes (*CLV3*, *WUS*, and *FIL*) across 3 cell types. (*K*) A comparison of relative levels of *CLV3, WUS*, and *FIL* transcripts, measured by qRT-PCR, in RNA samples derived from CLV3p, WUSp, and FILp cells respectively.

Description of Cell Type-Specific Fluorescent Markers. We introduced fluorescent reporters into the *ap1-1;cal1-1* background to differentially label 3 distinct cell types of the SAM stem cell niche. The *pCLV3*::*mGFP5-ER* was used to label cell types of the CZ (4). The *CLV3* expression is restricted to the CZ and the expression extends into the 4th layer starting from the tip (Fig. 1 *A* and *D*). *pWUS*::*mGFP5-ER* (*WUSCHEL* promoter driving the expression of endoplasmic reticulum localized-GFP) was used to label cells of the RM and it is expressed only in a few centrally-located cells of the L3 layers (Fig. 1 *B* and *E* and Fig. S3*D*). The *pFILAMENTOUSFLOWER* (*FIL*)::*dsRED-N7* (*FIL* promoter driving the expression of nuclear-localized dsRED) was used to label specific subsets of cells of the flower organ primordia located within the PZ (Fig. 1 *C* and *F*) (12). For simplicity, the 3 cell samples will be referred to as CLV3p, FILp and WUSp. The 3 fluorescent reporters do not express in all cell types of SAMs. Therefore, while collecting GFP positive protoplasts from CLV3p cells, we also collected GFP negative (CLV3n) protoplasts (Fig. S4). The CLV3n cell populations are expected to represent a mixture of SAM cell types that lacks the CLV3p cells.

RNA samples from 4 different protoplast populations (CLV3p, FILp, WUSp and CLV3n) were hybridized to the Affymetrix GeneChip ATH1 in biological replicates. Correlation coefficients close to 1.0 among the replicates indicated a high reproducibility of the experiments (Table S1). To estimate the extent of gene expression changes in response to the protoplasting method, we compared the gene expression patterns of protoplasted-*ap1-1;cal1-1* SAMs with nonprotoplasted-SAMs. Three hundred genes were found to respond to the protoplasting method. In the subsequent analysis these genes were not considered as cell-specific gene candidates (Table S2).

Cell Sample-Specific Expression Profiling Reveals Higher Sensitivity. The cell type-specific transcriptome analysis of *Arabidopsis* root cell types has revealed higher sensitivity than experiments with whole root samples (7). To assess a similar sensitivity increase for our datasets, we compared the detectable gene sets obtained from cell sample-specific expression profiling dataset (cell-sorted) with that of whole (cell-unsorted) *ap1-1;cal1-1* SAMs (Table S3). The comparison of cell-sorted data with that of the whole *ap1-1;ca1-1* SAMs revealed 952 genes that could only be identified in the cell type-specific transcriptome (Fig. 2*D*). This cell type-specific set includes *CLV3* (Fig. S5 and Table S4), *MEI2 C-Terminal RRM-like1* (*MCT1*) (Fig. 3*E* and Fig. S2), *B3-TF* (Fig. 3*H* and Fig. S2) and *JAGGED LATERAL ORGANS* (Fig. S5 and Table S4), which are expressed in small subsets of cells within the SAMs. We also compared the detectable gene sets from our cell sample-specific data with that of the pooled-microarray data of entire AtGenExpress developmental series of WT plants (Fig. 2*D* and *SI Text*) (7). This comparison yielded 1031 genes that were unique to cell sample-specific data and it includes *PUMILIO10* (Fig. 3*A*), *CLV3*, *MCT1* (Fig. 3*E*), *MCT2* (Fig. 3*B*) and *BLADE ON PETIOLE2* (Fig. S5 and Table S4), all of them are expressed in very few cells of the SAMs. The comparison of detectable genes in our cell sample-specific dataset with that

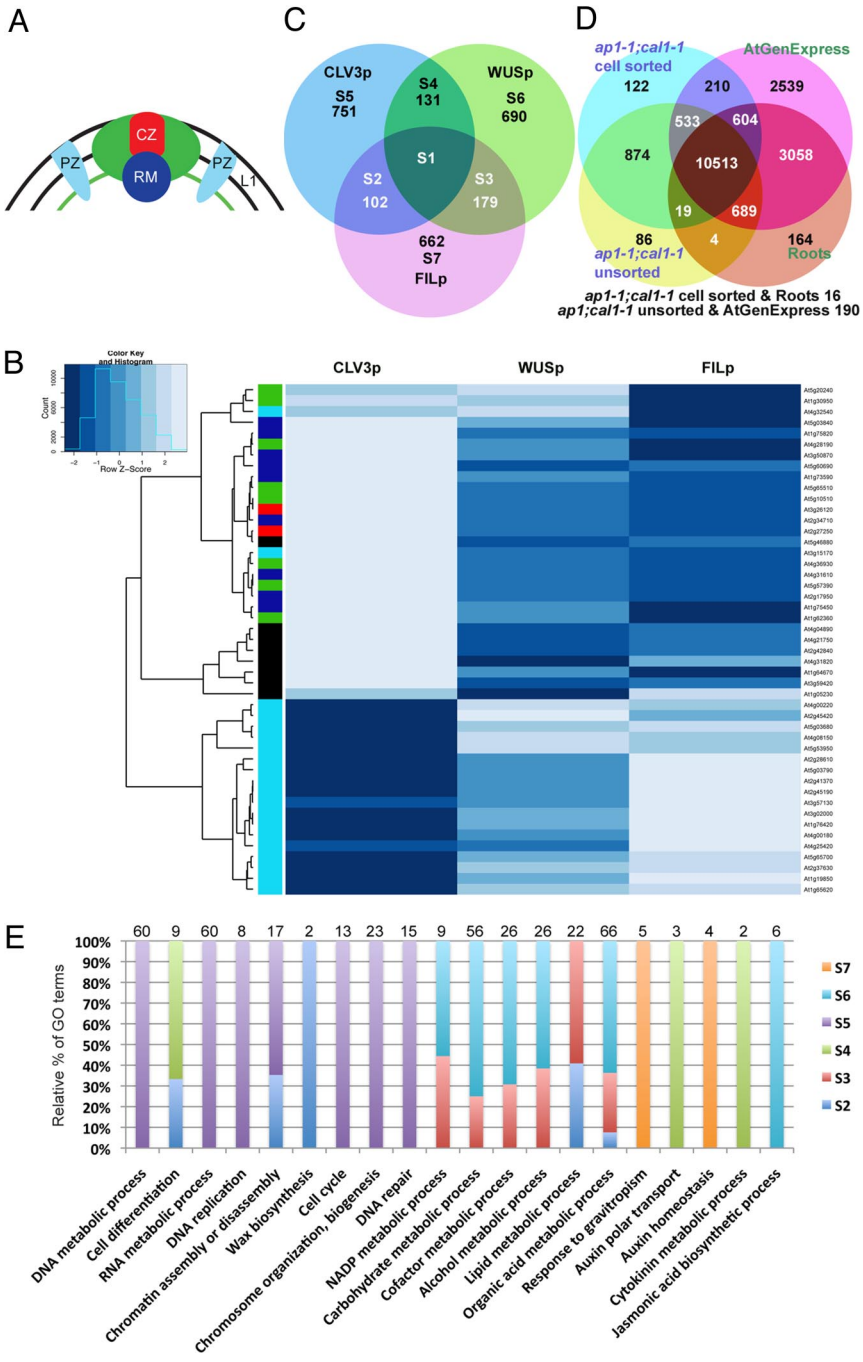

Fig. 2. Differential gene expression patterns of SAM cell types. (*A*) A sketch representing 5 regions of SAMs, the central zone narrow (CZ) (red), the CZ broad (green), the rib meristem (RM) (blue), the peripheral zone (PZ) (cyan), and the L1 layer (black). This sketch is a broad representation of different spatial patterns of characterized differentially-expressed genes. (*B*) Hierarchical clustering of 47 characterized differentially-expressed genes within the SAM, using the microarray data derived from 3 cell types (CLV3p, FILp, and WUSp). The color scheme used for representing clusters on the tree is same as the one used for representing different regions in *A*. (*C*) A 3-way comparison of all differentially-expressed genes enriched genes in CLV3p, WUSp, and FILp cell samples. The DEGs were classified into 6 sectors (*SI Text*). (*D*) A 4-way comparison of total number of genes detected (MAS5 present calls) in cell type-specific transcriptome (*ap1-1;cal1-1* cell sorted), the whole *ap1-1;cal1-1* apex (unsorted), the pooled microarray data of development series of WT plants from AtGenExpress study (AtGenExpress) and the cell type-specific data from *Arabidopsis* root tissue (roots). (*E*) Relative percentage of selected Gene Ontology (GO) groups identified in different DEG sectors. Note the number above each column represents a sum of total number of genes detected for a particular GO term in various sectors.

of the *Arabidopsis* roots revealed 3,915 genes specific to the root cell types, whereas 1,739 genes were specific to SAM cell types (Fig. 2*D* and *SI Text*) (3, 6). Taken together, the cell type-specific transcriptome, as expected, revealed higher sensitivity in identifying rare transcripts and genes that are unique to either the shoot or root cell-types.

Differential Expression Analysis and Validation of Microarray Data. To identify differences in gene expression programs among the individual cell types, we identified differentially-expressed genes (DEGs) (*SI Text*). Systematic comparisons among all 3 cell samples identified a union set of 2515 DEGs [$P < 0.01$ (Table S5 and *SI Text*)]. Next we generated 3 lines of evidence to validate the cell sample specific transcriptome data. First, we measured the relative abundance of transcripts of 3 marker genes (*CLV3*, *WUS*, and *FIL*), in isolated protoplasts by quantitative RT-PCR (qRT-PCR). The results showed an increased expression of the transcripts for *CLV3*, *WUS*, and *FIL* in the respective cell samples, which correlates well with the microarray expression data (Fig. 1 *J* and *K*). The detection of *WUS* transcripts in CLV3p cells suggested that the expression of 2 genes overlap with each other. We generated a double transgenic plant carrying *pCLV3*::*mGFP5-ER* and *pWUS*::*dsRED-N7* (*WUS-CHEL* promoter attached to nuclear-localized dsRED) to test whether the expression domains of *CLV3* and *WUS* overlap with each other. A high resolution microscopic analysis revealed that the 2 genes are expressed in overlapping sets of cells located in L3 layers of SAMs (Fig. S3 *A–I*). Although we detected high levels of *WUS* transcripts in CLV3p cells, however, a similar enrichment of *WUS* transcripts in CLV3p cells was not observed (Fig. 1 *J* and *K*). This could be due to the dilution of CLV3-expressing cells because of a

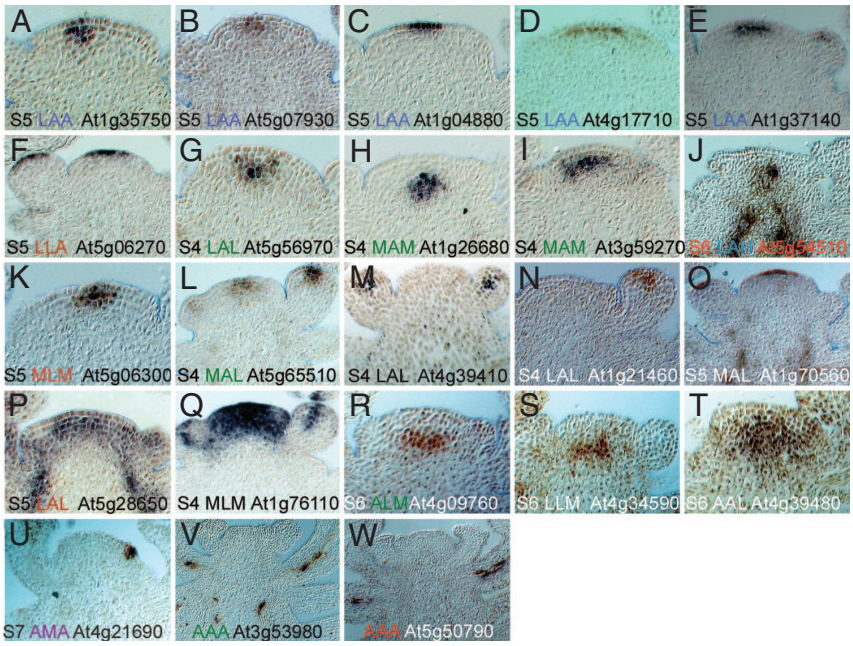

Fig. 3. Validation of differentially-expressed genes reveals gene expression domains within the WT SAMs. Shown are longitudinal sections of WT SAMs revealing RNA in situ hybridization signals of 23 genes that belong to different sectors and intensity interval clusters. The gene identification numbers, the DEG sectors and the intensity interval clusters are marked. Refer to Fig. S2 for additional views of expression patterns. For example, the expression pattern in *O* could also be seen in deeper layers of SAMs.

higher ratio of WUSp:CLV3p cells in regions where the 2 domains overlap. Enrichment of *WUS* transcripts in CLV3p cells, although the overlap is restricted to very few cells, could be because of higher levels of *WUS* expression in the most centrally-located cells of the *WUS* expression domain that overlap with the *CLV3* expression domain. Our whole-mount *WUS* RNA in situ expression patterns reveal that *WUS* is expressed in a graded fashion with higher levels of expression detected in the centrally-located cells (Fig. S3 *I* and *J*). Second, we tested the transcript abundance of 7 genes by qRT-PCR that appeared to be differentially-expressed among CLV3p and CLV3n cell samples and found that the relative transcript abundance in the respective cell types was in agreement with the microarray data (Fig. S4). Third, we analyzed the relative expression differences of genes for which RNA in situ expression patterns and promoter reporter expression data are available from earlier studies (Fig. 2*B*, Fig. S5, and Table S4). The relative enrichment of characterized differentially-expressed genes across cell samples was in agreement with our DEG analysis results (Table S5 and Fig. S5). Hierarchical cluster analysis grouped these genes largely according to their expression patterns observed on tissue sections, such as the PZ, the L1 layer, the CZ (includes narrow and broad) and the overlapping region between the CZ and the RM (Fig. 2 *A* and *B*).

Comparison of Differential Gene Expression Among 3 Cell Samples Reveals Unique and Overlapping Sectors of Gene Activity. We organized the set of 2515 DEGs into 3 subcategories by determining genes that exhibited a significant up-regulation in 1 of the 3 cell samples (CLV3p, WUSp, and FILp) relative to at least 1 of the 2 other cell samples. The 3-way Venn diagram representation of these 3 DEG lists revealed 7 possible overlap/uniqueness sectors (Fig. 2*C*, Table S5, and *SI Text*). To mine this dataset, we evaluated the distribution of characterized marker genes in the individual Venn diagram sectors. The sector S5 (*CLV3* expression domain, which excludes *WUS* and *FIL* expression domains) is expected to represent the central part of superficial cell layers (the L1 or the L2 or both the L1 and the L2) of the SAM and it includes *CLV3, AINTEGUMENTA-LIKE* (*AIL5*, *AIL6*, and *AIL7*) and *TERMINAL EAR LIKE1* (Table S5 and Table S4). The sector S4 (shared between *CLV3* and *WUS* expression domains, which excludes *FIL* domain) is expected to represent central part of the SAM including the superficial cell layers of the Rib-meristem and it includes *SPATULA*, *REPRODUCTIVE MERISTEM1*, *HANBA TARANU/MONOPOLE*, *CLAVATA1*, *WUS*, *SHOOTMERISTEMLESS*, *TERMINAL FLOWER1*, *CYTOKININ OXIDASE5*, *PIN FORMED1* (Table S5 and Table S4). The S6 (*WUS* expression domain, which excludes *CLV3* and *FIL* domains) is expected to represent deeper cell layers of differentiating region of the Rib-meristem. The S2 sector (shared between *CLV3* and *FIL* expression domains, which excludes *WUS* domains) is expected to represent superficial cell layers (the L1 or the L2 or both the L1 and the L2) of the entire SAM surface including differentiating cells of the organ primordia and it includes *ARABIDOPSIS CRINKLY4*, *ARABIDOPSIS THALIANA MERISTEM LAYER1*, *PROTODERMAL FACTOR 1* and *2*, and *BODYGUARD* (Table S5 and Table S4). The S7 sector (exclusive *FIL* expression domain) is expected to represent cells of the PZ including differentiating organ primordia and it includes *FIL*, *ASYMMETRIC LEAVES1* and *2*, *CUP SHAPED COTYLEDON3* and many such genes (Table S5 and Table S4). The S3 (shared between *FIL* and *WUS* expression domains, which excludes *CLV3* domain) is expected to represent a relatively broad SAM region encompassing the differentiating cells of the organ primordia and the deeper cell layers of the Rib-meristem, and *BREVIPEDICELLUS* is associated with this sector (Table S5 and Table S4). Because a large part of the CLV3n cell sample is expected to be a part of FILp and WUSp cell samples, it was not included in the DEG analysis. However, a side-by-side comparison of expression values of genes in CLV3n cell sample with other cell samples has enabled us in assessing the radial dimensions of expression domains of genes that are part of the central region of SAMs (Fig. S2 and Fig. S5). Taken together, our analysis demonstrates that the dataset is suitable for analyzing the gene expression programs enriched in distinct spatial domains of SAMs.

Subclassification of DEGs Based on Expression Intensity. The organization of SAMs has been described with the help of a limited set of molecular markers. New molecular markers are required to gain a better understanding of the spatial organization of SAMs. Therefore, we sought to identify markers for cell types of SAMs by mining the datasets obtained from DEG analyses. DEG analyses, however, provide information across a continuous range of expression levels. To predict genes that are only expressed in discrete subdomains of the SAM, we subclassified the identified DEGs by their expression

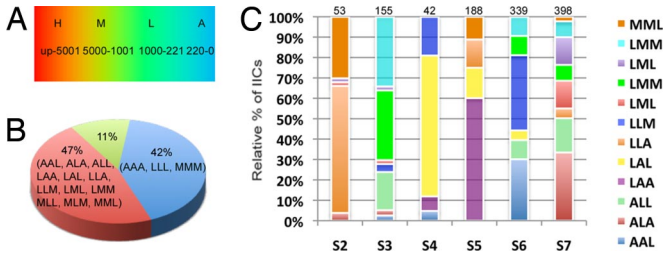

Fig. 4. Subclassification of DEGs by expression levels. (*A*) The gene expression levels of the identified DEGs were subdivided into 4 intensity levels, using the following intervals of the MAS5 normalized intensity data: A = absent (<220); L = low (220–1,000), M = medium (1,001–5,000) and H = high (>5,000). (*B*) A pie chart showing the relative distribution of selected groups of intensity interval clusters in the dataset. The sample order is defined as CLV3p, FILp, and WUSp, respectively (for example, AAA means absent in all 3, CLV3p, FILp, and WUSp samples). (*C*) The relative distribution of 12 intensity interval clusters that account for the 47% of differentially expressed gene are mapped onto individual DEG sectors derived from Fig. 2*C*. (The relative distribution of 49 intensity interval clusters that account for all DEGs can be found in Table S6). Above column is the total number of genes that are part of various intensity interval clusters (IICs) of a given sector. The relative distribution of different IICs, of a given sector, is expressed as percentage.

levels in the individual cell samples (Fig. 2*C* and 4*A*). For this, their normalized intensity values from the 3 cell samples, CLV3p, FILp and WUSp, were subgrouped into the 4 expression states absent (A), low (L), medium (M), and high (H) (Fig. 4*A* and *SI Text*). The 4 expression intervals for the 3 samples provide 81 possible intensity interval clusters (IICs), of which only 49 were observed in the dataset of the 2515 DEGs (Table S5 and Table S6). Approximately 42% of the DEGs could be classified into 3 IICs with the most uniform expression patterns, AAA, LLL and MMM (Fig. 4*B* and Table S6). The remaining 58% of DEGs received different intensity intervals, among cell types, and they could be organized into 2 subclasses (Fig. 4*B* and Table S6). The first one contained 12 IICs accounting for 47% of DEGs and the rest 11% of DEGs belonged to the remaining 34 IICs suggesting that their spatial expression is relatively restricted to specific subsets of cells (Fig. 4*B* and Table S6). Consistent with this hypothesis, a majority (40/47) of characterized differentially-expressed genes could be found in the latter 2 subclasses, suggesting that this approach can be applied to identify genes that are expressed in specific subsets of cells (Table S5 and Table S6).

Validation of DEGs by RNA in Situ Analysis Reveals Markers for Stem Cell Niche and Unique Expression Domains. Next, we mapped the 49 IICs onto the 6 overlap/uniqueness sectors of the DEG analysis (Fig. 4*C* and Table S6). This allowed us to predict genes with discrete spatial expression patterns and confirm their expression patterns by RNA in situ analysis (Fig. 3). For example, we hypothesized that the genes belonging to the LAA (Low in CLV3p, Absent in FILp and Absent in WUSp) cluster in the S4 and S5 sectors should exhibit an overlapping expression with the *CLV3* domain (Fig. 4*C* and Table S5). Indeed, the in situ experiments confirmed such an overlapping expression pattern within the *CLV3* domain (Fig. 3 *A–F* and Fig. S2). The subtle variations to the *CLV3* pattern could be observed, with gene expression restricted specifically to the L1 layer of the CZ (Fig. 3 *C* and *F*) or to the L2 layer of the CZ (Fig. 3*D*). The genes that are shared between *CLV3* and *WUS* domains could be identified in LAL, MAM, MAL, LAH or MLM cluster of S4 sectors (Fig. 3). These genes exhibited, the expression that overlaps with both the *CLV3* and the *WUS* domains (Fig. 3 *G–Q* and Fig. S2). The genes that were part of ALM, LLM and AAL clusters exhibited expression within the Rib-meristem (Fig. 3 *R–T*). Genes expressed in specific subsets of cells of the PZ could be found in the S7 sector (Fig. 3*U* and Fig. S2). A few genes that are part of the CLV3n cell sample, as expected, were excluded from 3 cell types and their expression was detected in the vasculature cells (Fig. 3 *V* and *W* and Fig. S2). Taken together, differential expression analysis and subsequent classification of DEGs based on expression levels can provide a better idea about their spatial expression patterns. However, the approach may not resolve finer differences in spatial expression patterns of genes that belong to the same IIC (Fig. 3 *K* and *Q*). This could be because of the inherent differences in gene expression levels and the rigid cut-off scale used for defining the intensity intervals. Nevertheless, our extensive in situ experiments demonstrate that the 49 IICs are a valuable data source for predicting spatial expression patterns. By using the markers that are expressed in distinct cell layers of the CZ (Fig. 3 *C* and *D*), we may be able to improve the spatial resolution and predictive capability of our expression map in the future.

Assessment of Overall Accuracy of the Technique and the DEG Analysis. To assess the accuracy of the technique, we considered a total of 70 documented differentially-expressed genes, including 23 expression patterns described in this study, whose spatial expression patterns could be judged with a fair degree of confidence. A comparison of DEG-predicted sectors of these genes with their observed spatial expression patterns on tissue sections revealed that 4 genes were incorrectly assigned to different DEG sectors and the other 4 genes were not identified as differentially-expressed, resulting in a combined error of 11% (Table S4). In contrast to our expectations, *BARELY ANY MERISTEM1*, *CUP SHAPED COTYLEDON2*, *REVOLUTA* and *ULTRAPETALA1* were not identified as DEGs, although a relative enrichment of these genes in expected cell samples could be detected (Table S5, Table S4, and Fig. S5). A notable exception is *CUP SHAPED COTYLEDON1*, which was associated with the S5 sector (CLV3p) instead of the S7 (FILp) (Table S4 and Table S5).

Overrepresentation of DNA Repair and Epigenetic Pathways in Stem Cells. It has been speculated, based on the organization of cell types, that the plant stem cell niches may share common properties with that of animal stem cell niches (13). However, molecular evidence to support this view is largely lacking because of the nonavailability of stem cell specific gene expression profile. To assess the molecular composition and pathways enriched stem cells, we performed enrichment analyses of Gene Ontology (GO) terms in our dataset (Fig. 2*E* and Table S7). First we tested the DEG sectors for overrepresented-GO terms that are characteristic for certain cell types of SAMs. The sector S2, which contained genes, expressed in the L1 layer was enriched with genes that are involved in wax biosynthesis ($P < 1.9 \times 10^{-2}$) and lipid metabolism ($P < 1.2 \times 10^{-2}$), which is consistent with one of the expected function of the L1 layer cells in secretion of epi-cuticular wax (14). As expected, the differentiating cells of the rib-meristem (S6) and differentiating cells of developing organs (S7) were over-represented with genes involved in various metabolic processes including that of carbohydrate metabolism, lignin deposition and photosynthetic genes (Fig. 2*E* and Table S7).

The sector S5, which is enriched in meristematic genes is over-represented with genes involved in DNA metabolism ($P < 1.17 \times 10^{-17}$), and DNA replication and repair ($P < 8.41 \times 10^{-6}$, 6.72×10^{-5}) (Fig. 2*E* and Table S7). This includes *MUTLI PROTEIN HOMOLOG 1* (*ATMSH1*), *MUTS HOMOLOG 2* (*MSH2*), *MUTS-LIKE PROTEIN 4* (*MSH4*), *MUTS HOMOLOG 6-2* (*MSH6-2*), *RADIATION SENSITIVE* (*ATRAD17*), *RADIATION SENSITIVE* (*ATRAD51*), *ARABIDOPSIS THALIANA BREAST CANCER ASSOCIATED RING1* (*ATBARD1*), *ARABIDOPSIS THALIANA BREAST CANNCER SUSCEPTIBILITIY1* (*ATBRCA1*), and *ARABIDOPSIS THALIANA TELOMERASE REVERSE TRANSCRIPTASE* (*ATTERT*), involved in telomere maintenance. The enrichment of both the enzymes of the mismatch repair and nonhomologous end-joining (NHEJ) DNA repair pathways suggest

PLANT BIOLOGY

that the SAM stem cells exhibit typical characteristics of cells experiencing stress (15). It is conceivable that error-free DNA replication is critical to prevent incorrect cellular amplification of mutations and amplification of stem cell daughters that carry double strand breaks, both can be deleterious to plant development.

Genes involved in chromosome organization and biogenesis ($P < 4.84 \times 10^{-7}$) were also over-represented in stem cells suggesting that the stem cell chromatin is maintained in a flexible state (Fig. 2*E* and Table S7). They include genes involved in HISTONE and DNA modifications such as centromeric *HISTONE H3*, *HISTONE ACETYL TRANSFERASE* (*HAM1*), *HISTONE DEACETYLASE 18* (*HD18*), *HISTONE LYSINE AND METHYL TRANSFERASES* (*SUVH4*, *SUVH9*, and *SUVR2*), *ARABIDOPSIS TRITHORAX-LIKE 1* (*ATX1*) and *SIRTUINS* (*SIR1* and *SIR2*), NAD-dependent deacetylases. Recent studies on murine embryonic stem cells (ES) have identified bivalent domains of both H3 lysine 27 methylation (a repressive chromatin mark) and H3 lysine 4 methylation (a chromatin mark that positively regulates transcription) within genes that encode developmentally important transcription factors. This suggested that the bivalent domains are responsible for keeping differentiation genes silent in ES cells, while keeping them primed for activation (16, 17). The enrichment of DNA and HISTONE modifying enzymes in stem cells of SAMs suggests that they might play a similar role in maintaining flexible chromatin to facilitate dynamic balance of gene expression. This can be tested, in future experiments, by profiling DNA and HISTONE modifications of individual cell types of SAMs with the method described here.

The genomic instability and changes in gene expression are regarded as hallmarks of the aging process in eukaryotes. A recent study, on mouse embryonic stem cells, has revealed that the mammalian deacetylase, Sir2 (SIRT1), in response to DNA damage, relocalizes to the sites of DNA breaks to mediate repair. The over-expression of SIRT1 has been shown to promote survival of mouse model of genomic instability and suppress age-related changes in transcription (18). The overrepresentation of *SIRTUINS* (*SIR1* and *SIR2*), pathways that respond to DNA damage and chromatin-modifying proteins suggests that the stem cells are under selective pressure to correct mutations.

Conclusions

We have described a method to generate a cell sample-specific gene expression map of SAMs. Our work has identified many genes with cell sample-specific expression profiles within the SAM stem cell niche. The gene expression patterns identified in this study can be used to refine the spatial organization of cell types of the SAMs. Identification of molecular signatures associated with these cell types may provide clues to their function. The markers for cells of the stem cell niche, identified in this study, can be a valuable resource in following the dynamic regulation of stem cell maintenance by cell–cell communication. The dataset is a valuable resource for guiding future functional analyses of stem cell enriched genes including evolutionarily conserved *PUMILIO* class of translational repressors and genes homologous to *LONELY GUY* (*LOG*) of rice, which has been shown to function in meristem development by regulating cytokinin biosynthesis (Fig. 3 *A* and *K*) (19, 20). More significantly, it is now possible to analyze cell–cell communication networks at a single cell type resolution, similar to the studies carried out in the *Arabidopsis* root system (21, 22). Elucidation of molecular networks at higher spatiotemporal resolution may provide a molecular framework to model cell–cell communication processes within the SAMs (23).

Materials and Methods

Transgenic Lines. The cell-type specific fluorescent reporter constructs used for expression profiling experiments have been described in the following studies, *CLV3*::*mGFP5-ER* (4) and *FIL*::*dsRED-N7* (12). *pWUS*::*mGFP5-ER* reporter line was assembled in pZP222 vector by using a 4.5-kb fragment upstream of *WUSCHEL* ORF and a 1.5-kb fragment downstream of the stop codon. The transgenic lines were generated using floral dip method (24). The double transgenic line expressing *CLV3*::*mGFP5-ER* and *WUS*::*dsRED-N7* has been described earlier (25). The transient silencing of *CLV3* was achieved by using the constructs described in earlier study (4).

Protoplasting of SAM Cells. Approximately 200 SAMs of 24-day-old *ap1-1;cal1-1* plants were harvested within 15 min and placed in protoplasting solution for ≈1 h and 15 min. The concentration and composition of cell wall digesting enzymes were optimized to obtain maximum protoplast yield (11, 26). Harvested shoot apices were incubated in protoplasting solution [Solution B = Solution A + 1.5% cellulase (YAKULT; catalog no. 203039), 1% Pectolyase (YAKULT pharmaceutical Ltd. Tokyo Japan, Catalog no. 202047) and 1% Hemicellulase (Sigma USA, catalog no. H2125)], within a 70 μM cell strainer placed in a small Petri-plate. Subsequent steps involved in harvesting protoplasts for FACS-mediated separation were carried out according to an earlier study (6). The modified protoplasting method yielded ≈150,000 to 200,000 fluorescently labeled protoplasts. The purity of sorting events was independently confirmed through microscopic observation of sorted protoplasts.

ACKNOWLEDGMENTS. We thank Barbara Walter (Institute of Inegrative Genome Biology, University of California, Riverside) for help with the FACS sorting and microarray hybridizations, Zhenhua Deng for help with qRT-PCR analysis, Nayana Hegde for help in generating marker lines, and Elliot Meyerowitz for providing *FIL*::*dsRED-N7* DNA construct, Nicholas Provart and Zhenbiao Yang for comments on the manuscript. DNA sequencing/quantitative PCR/Microarray data were generated by the Genomics Core at the Institute for Integrative Genome Biology at the University of California, Riverside. This work was funded by National Science Foundation Grant IOS-0718046 (to G.V.R.).

1. Morrison SJ, Spradling AC (2008) Stem cells and niches: Mechanisms that promote stem cell maintenance throughout life. *Cell* 132:598–611.
2. Dinneny JR, Benfey PN (2008) Plant stem cell niches: Standing the test of time. *Cell* 132:553–557.
3. Brady SM, et al. (2007) A high-resolution root spatiotemporal map reveals dominant expression patterns. *Science* 318:801–806.
4. Reddy GV, Meyerowitz EM (2005) Stem-cell homeostasis and growth dynamics can be uncoupled in the *Arabidopsis* shoot apex. *Science* 310:663–667.
5. Tucker MR, Laux T (2007) Connecting the paths in plant stem cell regulation. *Trends Cell Biol* 17:403–410.
6. Birnbaum K, et al. (2003) A gene expression map of the *Arabidopsis* root. *Science* 302:1956–1960.
7. Schmid M, et al. (2005) A gene expression map of *Arabidopsis thaliana* development. *Nat Genet* 37:501–506.
8. Ferrandiz C, Gu Q, Martienssen R, Yanofsky MF (2000) Redundant regulation of meristem identity and plant architecture by FRUITFULL, APETALA1 and CAULIFLOWER. *Development* 127:725–734.
9. Fletcher JC, Brand U, Running MP, Simon R, Meyerowitz EM (1999) Signaling of cell fate decisions by CLAVATA3 in *Arabidopsis* shoot meristems. *Science* 283:1911–1914.
10. Mayer KF, et al. (1998) Role of WUSCHEL in regulating stem cell fate in the Arabidopsis shoot meristem. *Cell* 95:805–815.
11. Birnbaum K, et al. (2005) Cell type-specific expression profiling in plants via cell sorting of protoplasts from fluorescent reporter lines. *Nat Methods* 2:615–619.
12. Heisler MG, et al. (2005) Patterns of auxin transport and gene expression during primordium development revealed by live imaging of the *Arabidopsis* inflorescence meristem. *Curr Biol* 15:1899–1911.
13. Scheres B (2007) Stem-cell niches: Nursery rhymes across kingdoms. *Nat Rev Mol Cell Biol* 8:345–354.
14. Suh MC, et al. (2005) Cuticular lipid composition, surface structure, and gene expression in *Arabidopsis* stem epidermis. *Plant Physiol* 139:1649–1665.
15. West CE, Waterworth WM, Sunderland PA, Bray CM (2004) Arabidopsis DNA double-strand break repair pathways. *Biochem Soc Trans* 32:964–966.
16. Bernstein BE, et al. (2006) A bivalent chromatin structure marks key developmental genes in embryonic stem cells. *Cell* 125:315–326.
17. Mikkelsen TS, et al. (2007) Genome-wide maps of chromatin state in pluripotent and lineage-committed cells. *Nature* 448:553–560.
18. Oberdoerffer P, et al. (2008) SIRT1 redistribution on chromatin promotes genomic stability but alters gene expression during aging. *Cell* 135:907–918.
19. Chen D, McKearin D (2005) Gene circuitry controlling a stem cell niche. *Curr Biol* 15:179–184.
20. Kurakawa T, et al. (2007) Direct control of shoot meristem activity by a cytokinin-activating enzyme. *Nature* 445:652–655.
21. Levesque MP, et al. (2006) Whole-genome analysis of the SHORT-ROOT developmental pathway in *Arabidopsis*. *PLoS Biol* 4:e143.
22. Gifford ML, Dean A, Gutierrez RA, Coruzzi GM, Birnbaum KD (2008) Cell-specific nitrogen responses mediate developmental plasticity. *Proc Natl Acad Sci USA* 105:803–808.
23. Jonsson H, et al. (2005) Modeling the organization of the WUSCHEL expression domain in the shoot apical meristem. *Bioinformatics* 21 (Suppl 1):i232–i240.
24. Clough SJ, Bent AF (1998) Floral dip: A simplified method for Agrobacterium-mediated transformation of *Arabidopsis thaliana*. *Plant J* 16:735–743.
25. Gordon SP, et al. (2007) Pattern formation during de novo assembly of the *Arabidopsis* shoot meristem. *Development* 134:3539–3548.
26. Guangyu C, Conner AJ, Christey MC, Fautrier AG, Field RJ (1997) Protoplast isolation from shoots of asparagus cultures. *Int J Plant Sci* 158:537–542.